International Journal of Mass Spectrometry 379 (2015) 46–51

Contents lists available at ScienceDirect

International Journal of Mass Spectrometry

journal homepage: www.elsevier.com/locate/ijms

Correction of dead time effects in laser-induced desorption time-of-flight mass spectrometry: Applications in atom probe tomography

Thomas Stephan[a,b,c,*], Philipp R. Heck[b,c], Dieter Isheim[d], Josiah B. Lewis[e,f]

[a] Department of the Geophysical Sciences, The University of Chicago, Chicago, IL, USA
[b] Chicago Center for Cosmochemistry, The University of Chicago, Chicago, IL, USA
[c] Robert A. Pritzker Center for Meteoritics and Polar Studies, The Field Museum, Chicago, IL, USA
[d] Northwestern University Center for Atom-Probe Tomography (NUCAPT), Department of Materials Science & Engineering, Northwestern University, Evanston, IL, USA
[e] Laboratory for Space Sciences, Washington University, St. Louis, MO, USA
[f] Physics Department, Washington University, St. Louis, MO, USA

ARTICLE INFO

Article history:
Received 11 October 2014
Received in revised form
11 December 2014
Accepted 17 December 2014
Available online 26 December 2014

Keywords:
Dead time correction
Time-of-flight mass spectrometry (TOF-MS)
Laser-induced desorption
Atom probe tomography (APT)

ABSTRACT

Dead time effects in time-of-flight secondary ion mass spectrometry are well known and can be corrected for using Poisson statistics. Laser-induced desorption, however, introduces nonlinearity in the evaporation process resulting in highly fluctuating signals that make proper dead time correction much more challenging. Here, we propose a modified dead time correction procedure that overcomes such obstacles using data from correlated detection events from different isotopes of a single element. Provided the signals are not affected by unresolved mass interferences, this dead time correction enables us to obtain meaningful isotope ratios as demonstrated for atom probe tomography data of carbon from nanodiamonds and of silicon.

1. Introduction

Any detector is able to reliably distinguish between different events only if they are separated from each other sufficiently either in time or in space. The duration a detector needs to recover after a counting event in order to be able to detect a second event following shortly afterwards is described as the dead time of the detector. It should be clarified that detector in this context describes the entire detection system typically consisting of several components such as the actual detector, typically a photomultiplier or microchannel plate, a discriminator that accepts signals as counting events or rejects them as electronic noise, and a time digitizer, which converts time intervals into digital representations.

In favorable cases, statistical approaches can be used to correct for dead time effects in order to calculate the signal intensities that an ideal detector with no dead time would have delivered. Dead time correction in time-of-flight mass spectrometry (TOF-MS) is complicated by the fact that signal intensities vary on very short time scales. However, such highly fluctuating signals can often be corrected for dead time effects as described in the literature [1]. Correction is possible since each measurement usually averages over a large number of ionization events that, except for statistical fluctuations, are uniform in ionization yield. This is typically fulfilled, e.g., in time-of-flight secondary ion mass spectrometry (TOF-SIMS) as long as the measurement is restricted to a homogeneous sample or sample region and neither sample properties nor primary ion beam intensity vary significantly during the analysis. Here, dead time correction works well and is now standard protocol during quantitative data evaluation [2–4]. An interlaboratory study involving 21 TOF-SIMS instruments has shown that this dead time correction is generally applicable and robust [5].

However, for some TOF-MS techniques, ionization yield is not constant and the dead time correction described by Stephan et al. [1] could not be applied. This is especially the case in techniques where laser-induced desorption is used, e.g., in laser desorption resonance ionization mass spectrometry (RIMS). As described by Savina et al. [6], the desorption process is nonlinear in laser

* Corresponding author at: Department of the Geophysical Sciences, The University of Chicago, Chicago, IL, USA. Tel.: +1 773 702 8856.
E-mail address: tstephan@uchicago.edu (T. Stephan).

http://dx.doi.org/10.1016/j.ijms.2014.12.006
1387-3806/

pulse energy, and moderate fluctuations lead to large variations in the desorbed particle flux. Desorption lasers are therefore often operated in a very low power regime, where particles are desorbed only occasionally, in order to avoid relatively powerful laser pulses that would release many particles in a single shot [6]. Very low count rates are the consequence, and measurement times have to be increased drastically to achieve sufficient counting statistics, if high precision is required.

This is also the case in atom probe tomography (APT), which combines field evaporation triggered by pulsing from a focused ultraviolet laser in a constant electric field with TOF-MS [7,8]. Using APT in order to measure isotope ratios in nanoparticles would be highly desirable in particular for cosmochemical applications, e.g., to study the origin of meteoritic nanodiamonds [8]. However, such data so far suffer from instrumental biases [8] among which dead time effects seem to play a major role. Therefore, most APT applications until now focused on the elemental composition of samples, where high accuracy is less crucial, as it was previously impossible to get useful isotope ratios.

However, the importance of multi-hit events causing dead time effects, also referred to as pile-up or detector saturation, for interpretation of mass spectra in APT has been recognized in the field. It has been identified already in 1978 that atom probe data do not directly give the true composition of a sample and that Poisson statistics could be applied for correction [9]. In 1984, Cerezo et al. developed a statistical correction without making any prior assumptions as to the distribution of ions per pulse [10]. In 1988, Menand et al. made a similar approach but made use of double counting events [11]. More recently, methods such as a contingency table approach have been employed to study correlations in field evaporation and to improve quantification of measured compositions [12].

Here, we present a dead time correction of APT isotope data using Poisson statistics but avoiding some of the deficiencies from previous studies and apply this correction to carbon and silicon data [8]. By using correlated counting events from isotopes of the same element, the method presented here allows correction of APT data from ion species that vary significantly in their evaporation behavior with some elements being more prone to evaporation in multiples than others.

2. Counting statistics

In the following, we will focus on the simple case, where for one laser pulse, only one ion per species can be detected, and different species are separated by a sufficient time gap so that they do not interfere with each other. From Eq. (8) in Stephan et al. [1],

$$ {}^{a}E = -N \cdot \ln\left(1 - \frac{a}{N}\right) \quad \text{and} \quad {}^{b}E = -N \cdot \ln\left(1 - \frac{b}{N}\right). \tag{1} $$

Here, ${}^{a}E$ and ${}^{b}E$ describe the corrected peak integrals or *true intensities* for two isotopes of an element E, whereas a and b represent the *measured intensities* for these isotopes, and N is the number of ionization events. It should be clarified here that, in general, the number of ionization events is smaller than the number of pulses from the desorption laser, if we assume that many laser pulses do not have the potential to cause ionization of the element of interest. This is different from TOF-SIMS, where each primary ion pulse is considered an ionization event, and N is a known quantity. For laser-induced desorption, N is unknown and may depend on the ion species. N is not the number of pulses in which ionization occurs; rather, it can be best described as the number of laser pulses where the conditions for formation of a given ion species are met. However, we can assume that N is identical for different isotopes of the same element and that isotope effects on desorption yields can be neglected.

2.1. The number of ionization events

If we now assume that detection of both isotope species is independent, the probability of detecting a correlated event, where both isotopes are detected in a single ionization event, is

$$ \frac{c}{N} = \frac{a}{N} \cdot \frac{b}{N}. \tag{2} $$

Here, c is the number of laser pulses for which both isotopes are detected. N can therefore be calculated as

$$ N = \frac{a \cdot b}{c}. \tag{3} $$

For the statistical error ΔN, one has to take into account that a and b are not independent from c. We therefore introduce

$$ a' = a - c \quad \text{and} \quad b' = b - c \tag{4} $$

as independent variables, since they are the number of counting events for both isotopes not including the number of correlated events given by c. Eq. (3) now becomes

$$ N = \frac{(a' + c)(b' + c)}{c}. \tag{5} $$

The statistical error ΔN now follows from the error propagation theorem as

$$ \Delta N = \sqrt{\left(\frac{b' + c}{c}\Delta a'\right)^2 + \left(\frac{a' + c}{c}\Delta b'\right)^2 + \left(\left(1 - \frac{a' \cdot b'}{c^2}\right)\Delta c\right)^2}. \tag{6} $$

Using the original variables a and b, this can also be written as

$$ \Delta N = \sqrt{\left(\frac{b}{c}\Delta a'\right)^2 + \left(\frac{a}{c}\Delta b'\right)^2 + \left(\frac{a + b - N}{c}\Delta c\right)^2}. \tag{7} $$

2.2. Peak integrals

Using Eq. (3), the peak integral ${}^{a}E$ from Eq. (1) can be calculated as

$$ {}^{a}E = -\frac{a \cdot b}{c} \cdot \ln\left(1 - \frac{c}{b}\right). \tag{8} $$

For calculation of the statistical errors, independent variables are needed

$$ {}^{a}E = -\frac{(a' + c)(b' + c)}{c} \cdot \ln\left(\frac{b'}{b' + c}\right). \tag{9} $$

Then, the statistical error becomes

$$ \Delta {}^{a}E = \sqrt{\left[\left(\frac{b' + c}{c} \cdot \ln\left(\frac{b'}{b' + c}\right)\right)\Delta a'\right]^2 + \left[\left(\frac{a' + c}{b'} + \frac{a' + c}{c}\ln\left(\frac{b'}{b' + c}\right)\right)\Delta b'\right]^2 + \left[\left(\frac{a' + c}{c} + \left(\frac{a' \cdot b'}{c^2} - 1\right)\ln\left(\frac{b'}{b' + c}\right)\right)\Delta c\right]^2}. \tag{10} $$

Using the original variables a and b, this can also be written as

$$ \Delta {}^{a}E = \sqrt{\left[\left(\frac{b}{c} \cdot \ln\left(1 - \frac{c}{b}\right)\right)\Delta a'\right]^2 + \left[\left(\frac{a}{b - c} + \frac{a}{c}\ln\left(1 - \frac{c}{b}\right)\right)\Delta b'\right]^2 + \left[\left(\frac{a}{c} + \left(\frac{a \cdot b}{c^2} - \frac{a + b}{c}\right)\ln\left(1 - \frac{c}{b}\right)\right)\Delta c\right]^2}, \tag{11} $$

which can be further simplified to

$$\Delta^a E = \sqrt{\left[\frac{^aE}{a}\Delta a'\right]^2 + \left[\left(\frac{a}{b-c} - \frac{^aE}{b}\right)\Delta b'\right]^2 + \left[\left(\frac{a}{c} + \frac{^aE}{a} + \frac{^aE}{b} - \frac{^aE}{c}\right)\Delta c\right]^2}. \quad (12)$$

2.3. Isotope ratios

In practical cases, we want to calculate isotope ratios from the measured peak integrals

$$\frac{^aE}{^bE} = \frac{\ln\left(1-\frac{c}{b}\right)}{\ln\left(1-\frac{c}{a}\right)} = \frac{\ln\left(\frac{b'}{b'+c}\right)}{\ln\left(\frac{a'}{a'+c}\right)}. \quad (13)$$

The statistical error can be expressed as

$$\Delta\left(\frac{^aE}{^bE}\right) = \sqrt{\left[\frac{c\cdot\ln\left(\frac{b'}{b'+c}\right)}{a'(a'+c)\left(\ln\left(\frac{a'}{a'+c}\right)\right)^2}\Delta a'\right]^2 + \left[\frac{c}{b'(b'+c)\cdot\ln\left(\frac{a'}{a'+c}\right)}\Delta b'\right]^2 + \left[\frac{\frac{\ln\left(\frac{b'}{b'+c}\right)}{a'+c} - \frac{\ln\left(\frac{a'}{a'+c}\right)}{b'+c}}{\left(\ln\left(\frac{a'}{a'+c}\right)\right)^2}\Delta c\right]^2}. \quad (14)$$

Using the original variables a and b, this can also be written as

$$\Delta\left(\frac{^aE}{^bE}\right) = \sqrt{\left[\frac{c\cdot\ln\left(1-\frac{c}{b}\right)}{a(a-c)\left(\ln\left(1-\frac{c}{a}\right)\right)^2}\Delta a'\right]^2 + \left[\frac{c}{b(b-c)\cdot\ln\left(1-\frac{c}{a}\right)}\Delta b'\right]^2 + \left[\frac{\frac{\ln\left(1-\frac{c}{b}\right)}{a} - \frac{\ln\left(1-\frac{c}{a}\right)}{b}}{\left(\ln\left(1-\frac{c}{a}\right)\right)^2}\Delta c\right]^2}, \quad (15)$$

which can be further simplified to

$$\Delta\left(\frac{^aE}{^bE}\right) = \sqrt{\left[\frac{^aE\cdot b}{^bE^2}\cdot\frac{\Delta a'}{a'}\right]^2 + \left[\frac{a}{^bE}\cdot\frac{\Delta b'}{b'}\right]^2 + \left[\frac{^aE\cdot b - a\cdot{}^bE}{^bE^2}\cdot\frac{\Delta c}{c}\right]^2}. \quad (16)$$

3. Experimental results and discussion

In order to evaluate the feasibility of the dead time correction according to Eqs. (13) and (16) for APT data, we applied the correction to carbon data obtained from synthetic nanodiamonds and to silicon data from silicon microtips [8]. In that study, $^{12}C/^{13}C$ ratios as well as $^{28}Si/^{29}Si$ and $^{28}Si/^{30}Si$ ratios that are apparently lower than expected were measured [8]. This was in part attributed to dead time effects, which leads to an undercount of the major isotopes ^{12}C and ^{28}Si compared to the less abundant isotopes ^{13}C, ^{29}Si, and ^{30}Si [8]. In addition to undercounting major isotopes, unresolved interference from hydride ions $^{12}CH^+$, $^{28}SiH^+$, and $^{29}SiH^+$ could lead to overestimated $^{13}C^+$, $^{29}Si^+$, and $^{30}Si^+$ signals. However, besides singly charged ions, carbon and silicon both also form doubly charged ions in APT. Since hydrides are not expected to form doubly charged ions and no major interferences are expected at the respective mass-to-charge-state ratios, using doubly charged ions can be advantageous for measuring carbon and silicon isotope ratios.

As mentioned above, we assumed for our dead time correction the simple case, where for one laser pulse, only one ion per species can be detected, and different species are separated by a sufficient time gap so that they do not interfere with each other. Modern APT instruments, however, allow for the detection of more than one ion with a given mass-to-charge-state ratio generated in a single laser pulse, though with a decreased detection efficiency for consecutive ions of the same species. In other words, the detector is not *dead* after being hit by an ion but has a decreased sensitivity for a certain amount of time. Since this reduced sensitivity is difficult to account for quantitatively, we counted multiple detections of one ion species only as single events. This required evaluation of single shot data and not just of spectra accumulated from a large number of laser pulses. Although disregarding ion detections might look like throwing away useful data, for the calculation of isotope ratios, we currently cannot make use of any additional information they might carry. Their detection can, however, still deliver valuable information about the three-dimensional distribution of the isotopes, since APT not only provides mass-to-charge ratios but also spatial information [7].

In some cases, data evaluation suffers from long tails of the respective mass peaks that even affects peaks at the following nominal mass. Sample preparation, material properties such as thermal conductivity, analytical conditions (laser energy and focus, pulse rate, and specimen temperature) can be optimized to minimize the formation of peak tails. For proper dead time correction, it is important to have a mass resolution sufficient to completely separate neighboring mass-to-charge-state ratios. While it is often sufficient to separate mass peaks by fitting them to some idealized shape, such peak deconvolution cannot be executed here since it could not be applied to single shot data. In cases where hydride interference cannot be excluded, the formation of doubly charged ions becomes very important for isotope measurements. Instrument parameters such as laser pulse energy and electric fields can be optimized in order to facilitate the formation of doubly charged ions [8,13].

3.1. Carbon

Synthetic detonation nanodiamonds (DNDs) and ultrananocrystalline diamonds (UNCDs) have been used as standards in an APT study of nanodiamonds from the Allende meteorite [8]. These synthetic standards are expected to have a $^{12}C/^{13}C$ ratio close to the terrestrial value of 89 and should be suited to evaluate the dead time correction described above.

From the previous study [8], five measurements showed sufficient mass resolution, short peak tails, as well as sufficient counts of doubly charged ions to allow for dead time correction of both singly and doubly charged carbon ion counts. Dead time corrected and uncorrected carbon isotope ratios for these measurements are shown in Fig. 1. In addition, Table 1 shows the number of laser pulses as well as the number of ionization events calculated from the data. As expected, the number of ionization events is smaller than the number of laser pulses: fewer than 0.35% of the laser pulses

Table 1
Carbon isotopes measured by APT in synthetic nanodiamonds as singly and doubly charged ions.[a]

Sample	UNCD 113215	DND 17620	DND 17626	DND 17969	UNCD 20026
Number of laser pulses	2.44×10^8	4.93×10^8	3.65×10^9	8.71×10^8	1.25×10^9
$N(^{12}C^+/^{13}C^+)$	$(9.0 \pm 0.8) \times 10^4$	$(1.7 \pm 3.8) \times 10^6$	$(8.8 \pm 4.1) \times 10^5$	$(1.1 \pm 0.5) \times 10^5$	$(1.9 \pm 0.4) \times 10^6$
$^{12}C^+/^{13}C^+$ (raw data)	10.3 ± 0.4	33 ± 3	53 ± 4	34 ± 3	81 ± 5
$^{12}C^+/^{13}C^+$ (corrected)	10.8 ± 0.4	33 ± 3	54 ± 4	35 ± 4	84 ± 5
$N(^{12}C^{++}/^{13}C^{++})$	$(1.4 \pm 0.2) \times 10^4$	$(1.7 \pm 0.2) \times 10^4$	$(2.8 \pm 0.5) \times 10^4$	$(1.4 \pm 0.2) \times 10^4$	$(1.8 \pm 0.1) \times 10^5$
$^{12}C^{++}/^{13}C^{++}$ (raw data)	71 ± 8	67 ± 8	66 ± 8	61 ± 9	57 ± 4
$^{12}C^{++}/^{13}C^{++}$ (corrected)	92 ± 12	83 ± 11	77 ± 11	75 ± 11	75 ± 7

[a] The number of ionization events N calculated according to Eqs. (3) and (7) is given for singly and doubly charged ions. The number of laser pulses is included for comparison. Ion ratios are calculated from raw data with no dead time correction and after dead time correction. Errors are 1σ statistical errors.

were above the ionization threshold for singly charged carbon ions, and fewer than 0.015% of the pulses were above the ionization threshold for doubly charged carbon ions. This is certainly in part due to the fact that the nanodiamonds were dispersed heterogeneously in the samples, but also reflects the high evaporation field requirements for carbon and instabilities of the field evaporation process that is thermally activated with the laser heating the sample surface to near the evaporation threshold [14,15].

Uncorrected peak ratios given in Table 1 in some cases differ significantly from values given by Heck et al. [8]. This is due to re-evaluation of the data using tighter peak interval definitions than in the previous study, trying to exclude some of the long peak tails that would make dead time correction impossible. However, variations in such interval definitions could not bring uncorrected peak ratios into agreement with expected isotope ratios.

After dead time correction, however, isotope ratios calculated from doubly charged ions are all within 2σ of the expected terrestrial ratio, whereas singly charged carbon ions yield $^{12}C/^{13}C$ ratios that are too low. This is probably due to interference from $^{12}C^1H^+$, which cannot be resolved from $^{13}C^+$. Hydride abundances seem to show huge variations between measurements leading to highly variable ratios of peaks measured at 12 and 13 u.

3.2. Silicon

Since some of the experiments described above were performed on nanodiamonds applied on silicon microtips (SMTs), we used data from these experiments to calculate silicon isotope ratios [8]. As for carbon, we expected isotope ratios for both singly and doubly charged silicon ions to be consistent with terrestrial values ($^{28}Si/^{29}Si = 19.7$, $^{28}Si/^{30}Si = 29.9$, and $^{29}Si/^{30}Si = 1.52$).

As for carbon, the measurements of silicon isotopes could suffer from unresolvable mass interferences. For $^{29}Si^+$ and $^{30}Si^+$, we expect interferences from $^{28}Si^1H^+$ and $^{29}Si^1H^+$, respectively. Since doubly charged ions appear at half nominal mass, one has to consider interferences for silicon isotopes with even mass numbers. Possible interferences for $^{28}Si^{++}$ at mass 14 u are $^{12}C^1H_2{}^+$ and $^{14}N^+$, while $^{12}C^1H_3{}^+$ and $^{14}N^1H^+$ could interfere with $^{30}Si^{++}$ at mass 15 u. However, since measurements were performed on silicon microtips, trace abundances of hydrocarbons and nitrogen should be less crucial, and we only expect major interferences from hydrides that should only affect singly charged silicon ions.

Fig. 2 shows the deviation of the uncorrected and dead time corrected doubly charged silicon ion ratios $^{29}Si^{++}/^{28}Si^{++}$ and $^{30}Si^{++}/^{28}Si^{++}$ from reference isotope ratios in per mill using the δ notation:

$$\delta\left(\frac{^aE}{^bE}\right) = \left(\frac{\left(\frac{^aE}{^bE}\right)_{\text{measured}}}{\left(\frac{^aE}{^bE}\right)_{\text{reference}}} - 1\right) \cdot 1000\ ‰\ . \tag{17}$$

Table 2 shows the number of laser pulses as well as the number of ionization events calculated from the data. As expected and similar to carbon, the number of ionization events is smaller than the number of laser pulses, demonstrating that in this case, fewer than

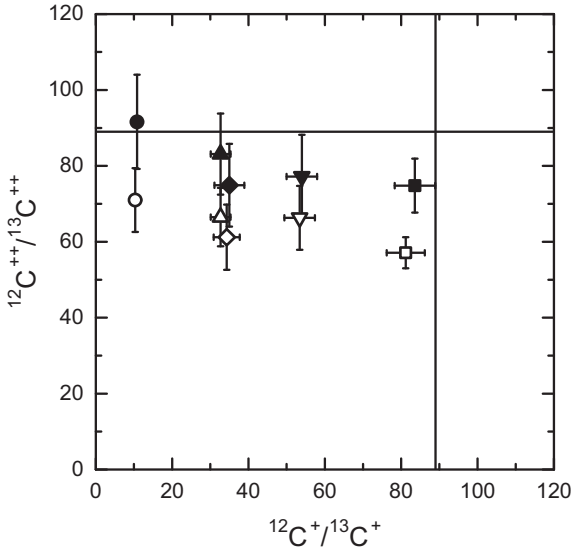

Fig. 1. Carbon isotope ratios calculated from measurements of singly and doubly charged carbon ions from synthetic nanodiamonds. Open symbols represent data from accumulated spectra not corrected for dead time effects. Data shown as solid symbols are dead time corrected. Error bars are 1σ statistical errors. Solid lines represent the expected $^{12}C/^{13}C$ ratio of 89.

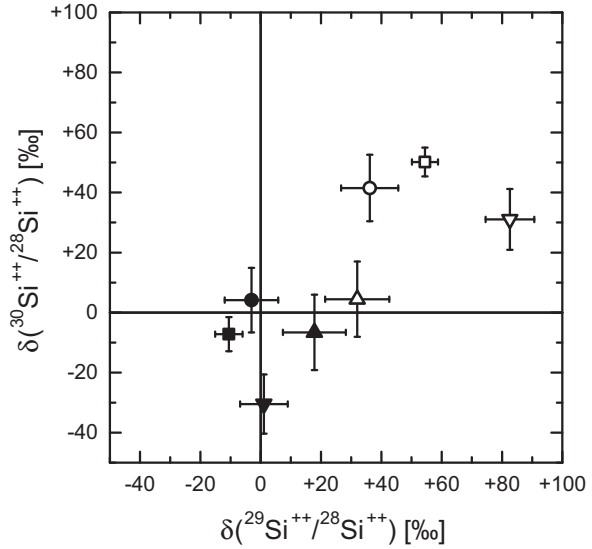

Fig. 2. Silicon isotope ratios calculated from measurements of doubly charged silicon ions from silicon microtips given in δ notation relative to expected terrestrial isotope ratios (solid lines). Open symbols represent data from accumulated spectra not corrected for dead time effects. Data shown as solid symbols are dead time corrected. Error bars are 1σ statistical errors.

Table 2
Silicon isotopes measured by APT in microtips as singly and doubly charged ions.[a]

Sample	SMT 113215	SMT 17134	SMT 17149	SMT 17153
Number of laser pulses	2.44×10^8	7.13×10^8	3.34×10^8	1.74×10^8
$N(^{28}Si^+/^{29}Si^+)$	$(1.2 \pm 0.2) \times 10^7$	$(1.4 \pm 0.2) \times 10^7$	$(1.3 \pm 0.2) \times 10^8$	$(1.9 \pm 1.1) \times 10^6$
$^{28}Si^+/^{29}Si^+$ (raw data)	16.3 ± 0.3	4.78 ± 0.06	19.0 ± 0.1	4.6 ± 0.2
$^{28}Si^+/^{29}Si^+$ (corrected)	16.3 ± 0.3	4.79 ± 0.06	19.0 ± 0.1	4.6 ± 0.2
$N(^{28}Si^+/^{30}Si^+)$	$(1.0 \pm 0.2) \times 10^7$	$(1.6 \pm 1.2) \times 10^7$	$(1.03 \pm 0.09) \times 10^8$	$(1.0 \pm 1.1) \times 10^6$
$^{28}Si^+/^{30}Si^+$ (raw data)	27.8 ± 0.5	22.9 ± 0.5	30.1 ± 0.2	19.2 ± 1.3
$^{28}Si^+/^{30}Si^+$ (corrected)	27.9 ± 0.6	23.0 ± 0.5	30.2 ± 0.2	19.3 ± 1.3
$N(^{29}Si^+/^{30}Si^+)$	$(7 \pm 6) \times 10^6$	–	$(1.2 \pm 0.5) \times 10^8$	–
$^{29}Si^+/^{30}Si^+$ (raw data)	1.71 ± 0.04	4.8 ± 0.1	1.59 ± 0.01	4.2 ± 0.3
$^{29}Si^+/^{30}Si^+$ (corrected)	1.71 ± 0.04	–	1.59 ± 0.01	–
$N(^{28}Si^{++}/^{29}Si^{++})$	$(3.3 \pm 0.1) \times 10^6$	$(1.40 \pm 0.03) \times 10^7$	$(6.8 \pm 0.4) \times 10^6$	$(2.40 \pm 0.05) \times 10^6$
$^{28}Si^{++}/^{29}Si^{++}$ (raw data)	19.0 ± 0.2	18.68 ± 0.08	19.1 ± 0.2	18.2 ± 0.1
$^{28}Si^{++}/^{29}Si^{++}$ (corrected)	19.8 ± 0.2	19.91 ± 0.09	19.4 ± 0.2	19.7 ± 0.2
$N(^{28}Si^{++}/^{30}Si^{++})$	$(3.5 \pm 0.1) \times 10^6$	$(1.60 \pm 0.06) \times 10^7$	$(8.6 \pm 0.7) \times 10^6$	$(3.06 \pm 0.09) \times 10^6$
$^{28}Si^{++}/^{30}Si^{++}$ (raw data)	28.7 ± 0.3	28.5 ± 0.1	29.8 ± 0.4	29.0 ± 0.3
$^{28}Si^{++}/^{30}Si^{++}$ (corrected)	29.8 ± 0.3	30.1 ± 0.2	30.1 ± 0.4	30.8 ± 0.3
$N(^{29}Si^{++}/^{30}Si^{++})$	$(3.6 \pm 0.6) \times 10^6$	$(1.16 \pm 0.09) \times 10^7$	$(5 \pm 1) \times 10^6$	$(1.7 \pm 0.1) \times 10^6$
$^{29}Si^{++}/^{30}Si^{++}$ (raw data)	1.51 ± 0.02	1.523 ± 0.009	1.56 ± 0.03	1.59 ± 0.02
$^{29}Si^{++}/^{30}Si^{++}$ (corrected)	1.51 ± 0.02	1.53 ± 0.01	1.56 ± 0.03	1.60 ± 0.02

[a] The number of ionization events N calculated according to Eqs. (3) and (7) is given for singly and doubly charged ion pairs ($^{28}Si/^{29}Si$, $^{28}Si/^{30}Si$, and $^{29}Si/^{30}Si$). The number of laser pulses is included for comparison. Ion ratios are calculated from raw data with no dead time correction and after dead time correction. Errors are 1σ statistical errors. Expected values for corrected isotope ratios are terrestrial values ($^{28}Si/^{29}Si = 19.7$, $^{28}Si/^{30}Si = 29.9$, and $^{29}Si/^{30}Si = 1.52$).

40% of the laser pulses could generate singly charged silicon ions, and fewer than 3% of the pulses were above the ionization threshold for doubly charged silicon ions. However, these numbers vary a lot among different runs as they depend on the sample properties and analytical conditions. In some cases, formation of doubly charged ions is even favored compared to formation of singly charged ions.

With three stable isotopes, silicon, in principle, enables evaluating three different isotope pairs. However, isotopic abundances of ^{29}Si and ^{30}Si are both below 5%, and correlated counting events for these isotopes are quite rare. In two cases (SMT 17134 and SMT 17153), there were no correlated counting events measured for $^{29}Si^+$ and $^{30}Si^+$ at all. In such cases, dead time correction cannot be applied. However, numbers of ionization events N for singly charged ion pairs $N(^{28}Si^+/^{29}Si^+)$, $N(^{28}Si^+/^{30}Si^+)$, and also for $N(^{29}Si^+/^{30}Si^+)$, when it could be determined, agree reasonably well within statistical errors. The same is true for doubly charged ion pairs $N(^{28}Si^{++}/^{29}Si^{++})$, $N(^{28}Si^{++}/^{30}Si^{++})$, and $N(^{29}Si^{++}/^{30}Si^{++})$. However, some discrepancies were observed, which might be due to some mass interferences that could have different evaporation thresholds in APT. In general, these discrepancies seem to be larger for singly charged ion pairs than for doubly charged ion pairs.

Corrected isotope ratios for the singly charged silicon ions (Table 2) clearly indicate that dead time effects are not the major reason for deviations of the isotope ratios from expected values. As in the case of carbon, we attribute this mainly to interferences from hydrides, which again show high variability. Doubly charged silicon ions after dead time correction, however, yield isotope ratios that are all within 2σ of the expected terrestrial ratios, except for one outlier, which is still within 3σ.

4. Conclusions

Correction of dead time effects in laser-induced desorption TOF-MS like, e.g., in APT is complicated by the nonlinearity of the desorption process, which leads to large variations of ionization yields during a typical measurement. Dead time correction following the general concept according to Stephan et al. [1], but using single shot data and taking into account correlated counting events from isotopes of the same element, can be used to mitigate these effects. However, this dead time correction only works if the respective mass peaks do not suffer from unresolved interferences. Due to the limited mass resolving power of current APT instruments and the possibility of unresolved interfering hydride peaks, using doubly charged ion signals can be advantageous to obtain accurate isotope ratios. Performing such measurements at laser pulse energies and field evaporation voltages that facilitate the formation of doubly charged ions can therefore be desirable. The correction presented here unlocks the full potential of APT regarding isotope analysis in small volumes or nanoparticles. This work has tremendous potential for isotope studies at a previously unreachable spatial dimension—the atomic scale.

Future investigations will show if the dead time correction laid out in this study could also be applied to other laser-induced desorption TOF-MS techniques like, e.g., laser desorption RIMS.

Acknowledgements

We thank M.J. Pellin and C. Floss for helpful discussions. We appreciate thoughtful comments by two anonymous reviewers. This work was supported by NASA through grants NNX09AG39G (T.S.), NNX11AG77G (P.R.H.), NNX13AF53G (J.B.L.), and NNX14AP15H (J.B.L.), and by a grant from the Tawani Foundation (P.R.H.). The LEAP tomograph at NUCAPT was purchased and upgraded with funding from NSF-MRI and ONR-DURIP programs. Instrumentation at NUCAPT was supported by the Initiative for Sustainability and Energy at Northwestern. This research made use of the EPIC facility and Shared Facilities at Northwestern University's Materials Research Science and Engineering Center, supported by the MRSEC program (DMR-0520513 and 1121262) of NSF. P.R.H. thanks Cameca Instruments, Inc., for access to their LEAP tomograph.

References

[1] T. Stephan, J. Zehnpfenning, A. Benninghoven, Correction of dead time effects in time-of-flight mass spectrometry, J. Vac. Sci. Technol. A 12 (1994) 405–410.
[2] T. Stephan, TOF-SIMS in cosmochemistry, Planet. Space Sci. 49 (2001) 859–906.
[3] M.R. Keenan, V.S. Smentkowski, J.A. Ohlhausen, P.G. Kotula, Mitigating dead-time effects during multivariate analysis of ToF-SIMS spectral images, Surf. Interface Anal. 40 (2008) 97–106.
[4] G. Holzlechner, M. Kubicek, H. Hutter, J. Fleig, A novel ToF-SIMS operation mode for improved accuracy and lateral resolution of oxygen isotope measurements on oxides, J. Anal. At. Spectrom. 28 (2013) 1080–1089.

[5] J.L.S. Lee, I.S. Gilmore, M.P. Seah, Linearity of the instrumental intensity scale in TOF-SIMS – a VAMAS interlaboratory study, Surf. Interface Anal. 44 (2012) 1–14.
[6] M.R. Savina, M.J. Pellin, C.E. Tripa, I.V. Veryovkin, W.F. Calaway, A.M. Davis, Analyzing individual presolar grains with CHARISMA, Geochim. Cosmochim. Acta 67 (2003) 3215–3225.
[7] T.F. Kelly, D.J. Larson, Atom probe tomography 2012, Annu. Rev. Mater. Res. 42 (2012) 1–31.
[8] P.R. Heck, F.J. Stadermann, D. Isheim, O. Auciello, T.L. Daulton, A.M. Davis, J.W. Elam, C. Floss, J. Hiller, D.J. Larson, J.B. Lewis, A. Mane, M.J. Pellin, M.R. Savina, D.N. Seidman, T. Stephan, Atom-probe analyses of nanodiamonds from Allende, Meteorit. Planet. Sci. 49 (2014) 453–467.
[9] T.T. Tsong, Y.S. Ng, S.V. Krishnaswamy, Quantification of atom-probe FIM data and an application to the investigation of surface segregation of alloys, Appl. Phys. Lett. 32 (1978) 778–780.
[10] A. Cerezo, G.D.W. Smith, A.R. Waugh, The FIM100 – performance of a commercial atom probe system, J. Phys. Colloq. 45 (1984), C9-329–C9-335.
[11] A. Menand, T. Al Kassab, S. Chambreland, J.M. Sarrau, Atom-probe study of aluminium–lithium alloys, J. Phys. Colloq. 49 (1988), C6-353–C6-358.
[12] D.W. Saxey, Correlated ion analysis and the interpretation of atom probe mass spectra, Ultramicroscopy 111 (2011) 473–479.
[13] D.R. Kingham, The post-ionization of field evaporated ions: a theoretical explanation of multiple charge states, Surf. Sci. 116 (1982) 273–301.
[14] J.H. Bunton, J.D. Olson, D.R. Lenz, T.F. Kelly, Advances in pulsed-laser atom probe: instrument and specimen design for optimum performance, Microsc. Microanal. 13 (2007) 418–427.
[15] F. Vurpillot, J. Houard, A. Vella, B. Deconihout, Thermal response of a field emitter subjected to ultra-fast laser illumination, J. Phys. D: Appl. Phys. 42 (2009) 125502 (7 pp).